# Astrometric and Photometric Data Fusion for Mass and Surface Material Estimation using Refined Bidirectional Reflectance Distribution Functions-Solar Radiation Pressure Model

**Richard Linares and John L. Crassidis**
*University at Buffalo*
**Charles J. Wetterer and Keric A. Hill**
*Pacific Defense Solutions*
**Moriba K. Jah**
*Air Force Research Laboratory*

**CONFERENCE PAPER**

This paper studies the inference of space object mass, which is made possible due to the coupled influence of solar radiation pressure (SRP) acceleration on the orbit of satellites and their observed brightness. This effect takes time to be observed in optical angle measurements given the combination of a priori kinematic state uncertainties and the magnitude of this effect relative to them and the sensor data noise. Therefore, multiple nights of observations are typically required to extract this "weak" signal from collected measurements. From angles data alone, only effective albedo-area-to-mass can be estimated since this term appears in the SRP acceleration equation, but when photometric data is fused with the astrometric angle measurements, it provides observability of, and thus constrains, the albedo-area estimates. This inferred constraint makes mass the most open degree of freedom and thus the fused data eventually informs the filter of the mass. The observability of albedo-area products is provided by the photometric brightness measurements, since the brightness of the space object is a strong function of the albedo-areas. However, the relationship between the albedo-areas and both the photometric return and SRP involves knowledge of the Bidirectional Reflectance Distribution Function (BRDF) for the surface of the space object. If the BRDF in the photometric measurement model and the BRDF in the SRP model are not consistent with each other, then the resulting estimated albedo-areas and mass are inaccurate and biased. This work studies the use of physically consistent BRDF-SRP models for mass estimation. Simulation studies are used to provide an indication of the benefits of using these new models. An unscented Kalman filter approach that includes BRDF and mass parameters in the state vector is used. The full set of estimated parameters includes position, velocity, attitude, angular rates, mass, exponential factor (parameter in Ashikhmin-Shirley BRDF related to sharpness of specular reflection), specular coefficient and diffuse coefficient. The challenge of adding these additional parameters is the fact that they are constrained, where all must be positive and the specular and diffuse coefficients must be less than unity. Two approaches are adopted to account for the constraints; the first approach projects the sigma points onto the constraint boundary if any violate the constraints on the parameters, and the second approach defines proxy parameters that are unconstrained version of the original parameters. The results for estimating mass are promising and show that the addition of consistent BRDF-SRP models benefits the estimation process.

## 1. INTRODUCTION

Deep space optical surveys of near geosynchronous (GEO) objects have identified a class of high area-to-mass ratio (HAMR) objects [1]. The exact characteristics of these objects are not well known and their motion pose a collision hazard with GEO objects due to the solar radiation pressure (SRP) induced, large variations of inclination and eccentricity. These objects are typically non-resolved and difficult to track due to dim magnitude and dynamic mismodeling. Therefore, characterizing the large population of HAMR objects in GEO orbits is required to allow for a better understanding of their origins, and the current and future threats they pose to the active space object (SO) population.

For establishing unique identification and discrimination of SOs, past researchers have searched for defining attributes that are unique to a given SO. These attributes can then be used to study classes of objects or at the very least correlate observations. An obvious attribute that can be assigned to an SO is its orbital state. Reference [2] studies the process of correlating a sequence of optical measurements to a given SO using constraints on the orbital states derived from the measurements. Although orbital states do provide an attribute to identify an SO, for the case of HAMR objects and objects with sparse observations it may be difficult to identify an SO with just this attribute.

In order to understand the nature and eventually the origin of these objects, physical characteristics such size, shape and material are required. These characteristics can serve as information on the shape and the attitude motion of a debris piece. They can be obtained from existing data sources such as photometric and astrometric data [3]. To investigate the surface material properties reflectance spectroscopy data can be gathered [4]. Reflectance spectroscopy or multi-band photometric data can be used to study non-resolved debris objects and determine their material composition [5]. The measurements made from debris objects can be compared to laboratory derived observations to determine material composition of the debris [6–8]. The photometric return depends on a number of parameters such as shape, size, material and observation geometry. Therefore, extracting material composition is difficult. Reference [9] studies the light curves of different uncontrolled SOs. From this study it is clear that there are unique features in these light curves. But reflectance parameters and albedo estimates may also provide useful attributes. Size estimates have been derived in the past using radar measurements [10], but for objects in higher orbits these types of measurements may not be available. Reference [11] develops a technique for estimating the intrinsic but rough size and albedo estimates of orbital fragmentation debris from optical measurements. These albedo values provide a very useful attribute, but the estimation technique assumes that the objects are spherical in shape. This assumption limits the accuracy of this method.

Features may also exist in the light curve measurements. For example some objects have been identified by the shape and features in their light curves. Reference [12] shows how glint data can be used to determine the solar panel off-set and improve the detectability of SOs. Glint data however is very much a function of the geometry and orientation of the SO, since glint events only occur at given reflection angles. Therefore, to process this data attitude and shape must be accounted for in the estimation process. Reference [12] does not use estimation techniques to account for the attitude dependency, but rather makes qualitative conclusions from glint data. Also Ref. [13] uses optimal control methods to determine reachability and correlate observations; knowledge of mass can greatly assist in these types of calculations.

Estimating the dynamic characteristics of a HAMR object using light curve and astrometric data can allow for mass parameters to be observable. Estimating mass for HAMR objects can help in the development of a detailed understanding of the origin and dynamics of these objects. It has been shown that the SRP albedo area-to-mass ratio, $C_rA/m$, is observable from angles data [14] through the dynamic mismodeling of SRP forces. Reference [14] conducts a study with simulated and actual data to quantify the error in the estimates of $C_rA/m$ and good performance is found using data spanning over a number of months. Also Ref. [15] shows that orbital, attitude and shape parameters can be recovered with sufficient accuracy using a multiple-model adaptive estimation approach coupled with an Unscented Kalman Filter (UKF). This approach works reasonably well but requires that the area-to-mass ratio be known a priori. The purpose of this work is to show that since $C_rA/m$ is observable from angles data and shape/albedo properties are observable from photometric data, then by fusing these data types mass can be extracted with reasonable accuracy.

The area-to-mass ratio of a space object can also provide an attribute. This ratio is very important for predicting the orbital motion of the SO under the influence of SRP. Since SRP is the primary nonconservative disturbance force for GEO objects it is a very important dynamical parameter for this class of objects. If the albedo of the object is known it may be possible to determine the mass from this parameter. A similar approach has been applied to low-Earth orbiting objects using the drag ballistic coefficient [16]. Knowing the mass of a space object can be very valuable. For example one can examine breakup fragments by determining the masses of each fragment [17]. This work will look at methods for determining the mass of an SO from photometric and astrometric data sources.

The organization of this paper is as follows. First, the methods used to recover mass are discussed. Then the models used for SO shape, orbital dynamics and attitude dynamics are discussed. Following this a description of the measurement models used in this paper is given. Next, a review of the constrained UKF approach is provided. Finally, simulation results of the mass and albedo-area estimation approach are provided.

## 2. DETAILS OF APPROACH

The mass estimation approach used in this paper depends on the fusion of the astrometric and photometric data. Since both of these data sources have an albedo-area dependency then mass can be separated from albedo-area through data fusion. For example consider the following simplified relationships for the acceleration and observed flux of a diffuse sphere:

$$\mathbf{a}_{SRP} = -\frac{C_r A}{m}\frac{F_{sun}}{c}\hat{\mathbf{L}} \tag{1a}$$

$$F_{flux} = C_{diff} A \frac{F_{sun0}}{\pi} \left( \frac{1+\cos\alpha}{2} \right) \tag{1b}$$

where $C_r$ is the reflectance coefficient of the sphere, $A$ is the sphere's cross sectional area, $m$ is the mass, $F_{\text{sun}}$ is the total solar flux over all wavelengths, $c$ is the speed of light, $C_{diff}$ is the diffuse coefficient of the surface, $F_{\text{sun0}}/\pi$ represents the diffuse BRDF with $F_{\text{sun0}}$ the solar flux through the band pass of the sensor, and $\alpha$ is the phase angle. As mentioned previously, light curve data (Eq. (1b)) is sensitive to $C_{diff}A$ and angles data (Eq. (1a)) is sensitive to $C_rA/m$. The $C_r$ coefficient is a function of the $C_{diff}$ of the SO surface. In general, $C_r = 1 + r$ for the cannonball model [14] where r is a modeling parameter related to the albedo. Therefore, to allow for mass to be separated from area, an estimate of albedo must be determined. Note that $r$ and $C_{diff}$ are not the same and rather $r$ is used to model the effect of $C_{diff}$ on the SRP. It is shown in Ref. [18] that $C_r = 1 + 2C_{diff}/3$ for a diffuse sphere and $C_r = 1 + 4C_{diff}/9$ for a diffuse flat plate assuming Lambert's cosine law with the normal direction aligned with the Sun direction.

From Eq. (1) and the relationship between $C_r$ and $C_{diff}$, it is clear that mass separated from area highly depends on the assumptions made about shape and surface reflection. Also it is clear that brightness and the SRP force are related by the physics that they model. Therefore, to obtain realistic and reliable estimates for mass both the SRP and light curve models must be physically consistent. Toward this end a general SRP model is defined as

$$\mathbf{a}_{SRP} = -\sum_{k=1}^{N_{facets}} \int_0^{\infty} \frac{F_i(\lambda) A_k f_k \left( \hat{\mathbf{L}} \cdot \hat{\mathbf{N}}_k \right)_+}{m_{so} c} \left( \hat{\mathbf{L}} + \left( \int_0^{2\pi} \int_0^{\pi/2} f_r \cos\theta_r \hat{\mathbf{V}} d\theta_r d\phi_r \right)_k \right) d\lambda \tag{2}$$

where this model calculates the acceleration due to $N_{facet}$ facets. The terms $A_k$, $f_k$, and $F_i(\lambda)$ are the area of the $k^{\text{th}}$ facet, fraction of facet that is illuminated, and the wavelength dependent solar flux respectively. Additionally, $(x)_+ = xH(x)$ where $H(x)$ is the Heaviside step function which is unity for positive values and zero elsewhere. The BRDF ($f_r$) defines how light is reflected from an opaque surface with a given surface normal direction ($\hat{\mathbf{N}}_k$) based on a light source in the $\hat{\mathbf{L}}$ direction. Finally each differential $d\theta_r d\varphi$ spherical element of outing light rays has a $\hat{\mathbf{V}}$ vector defining the direction of the acceleration due to ray exiting through this spherical element. Then the acceleration can be calculated by defining $f_r$ depending on the surface properties and then evaluating the integral in Eq. (2).

### 2.1 Shape Model

The shape model considered in this work consists of a finite number a flat facets. For curved surfaces this model becomes more accurate as the number of facets is increased. Each facet has a set of three basis vectors ($\mathbf{u}_n^B, \mathbf{u}_u^B, \mathbf{u}_v^B$) associated with it as defined in Figure 1(a). The unit vector $\mathbf{u}_n^B = \hat{\mathbf{N}}$ points in the direction of the outward normal to the facet, and the vectors $\mathbf{u}_u^B$ and $\mathbf{u}_v^B$ are in the plane of the facet. The notation superscript $B$ denotes that the vector is expressed in body coordinates. The SOs are assumed to be rigid bodies, so the unit vectors $\mathbf{u}_n^B$, $\mathbf{u}_u^B$ and $\mathbf{u}_v^B$ do not change in time since they are expressed in the body frame.

The light curve and the SRP models discussed in the next sections require that these vectors be expressed in inertial coordinates. Since the SO body is rotating, these vectors will change inertially. The body vectors can be rotated to the inertial frame by the standard attitude mapping given by

$$\mathbf{u}_k^B = A\left(\mathbf{q}_I^B\right)\mathbf{u}_k^I \quad k = u, v, n \tag{3}$$

where $A\left(\mathbf{q}_I^B\right)$ is the attitude matrix mapping the inertial frame to the body frame using the quaternion parameterization. The superscript $I$ denotes that a vector is expressed in inertial coordinates. The unit vector $\mathbf{u}_{\text{sun}}^I = \hat{\mathbf{L}}$ points from the SO to the Sun direction, and the unit vector $\mathbf{u}_{\text{obs}}^I = \hat{\mathbf{V}}$ points from the SO to the observer as shown in Figure 1(a). The vector $\mathbf{u}_{\text{h}}^I = \hat{\mathbf{H}}$ is the normalized half vector between $\mathbf{u}_{\text{sun}}^I$ and $\mathbf{u}_{\text{obs}}^I$ also shown in Figure 1(a). This vector is also known as the Sun-SO-Observer bisector and has an angle $\alpha$ from the normal ($\cos\alpha = \hat{\mathbf{N}}_k \cdot \hat{\mathbf{H}}$). Each facet has an area $A_k$ associated with it. Once the number of facets has been defined and their basis vectors are known, the areas $A_k$ define the size and shape of the SO.

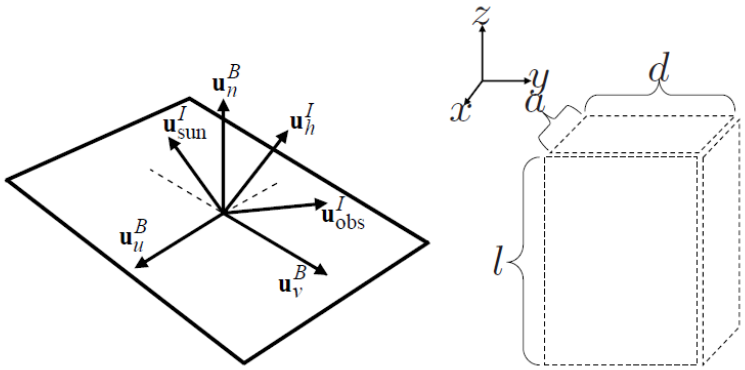


(a) Geometry of Reflection (b) Cuboid Shape Model

**Figure 1. Geometry and Shape Description**

For the development of the measured light curve data, faceted SO rectangular cuboid shape models as shown in Figure 1(b) are used. The rectangular cuboid model is described by three parameters, *l*, *a*, and *d*, which are the length, width and height, respectively.

### 2.2 Review of Bidirectional Reflectance Distribution Functions

A number of bidirectional reflectance distribution functions (BRDFs) exist in literature. These models are based on the BRDF that models light distribution scattered from the surface due to the incident light. The BRDF at any point on the surface is a function of two directions, the direction from which the light source originates and the direction from which the scattered light leaves the observed the surface. These models include Ashikhmin-Shirley [19], a simplified Blinn-Phong [20] and Cook-Torrance [21]. The BRDF models how light energy reflects off of surfaces and how this reflected energy is distributed.

The model in Ref. [19] decomposes the BRDF into a specular component and a diffuse component. The two terms sum to give the total BRDF:

$$\rho_{total}(i) = \rho_{spec}(i) + \rho_{diff}(i) \tag{4}$$

The diffuse component represents light that is scattered independent of the angle of incident light, and the specular component represents light that is concentrated about some direction (mirror-like). Reference [19] develops a model for continuous arbitrary surfaces but simplifies for flat surfaces. This simplified model is employed in this work as shape models are considered to consist of a finite number of flat facets. Therefore, the total observed brightness of an object becomes the sum of the contribution from each facet:

$$f_r = \left(dR_d + sR_s\right) \tag{5}$$

which depends on the diffuse bidirectional reflectance ($R_d$) and the specular bidirectional reflectance ($R_s$) and the fraction of each to the total ($d$ and $s$ respectively where $d + s = 1$). These bidirectional reflectances are calculated differently for the various models. In each model, however, $\rho$ is the diffuse reflectance ($0 \le \rho \le 1$), and $F_0$ is the specular reflectance of the surface at normal incidence ($0 \le F_0 \le 1$). To be used as a prediction tool for brightness and radiation pressure calculations, an important aspect of the BRDF is energy conservation. For energy to be conserved, the integral of the BRDF times cos ($\theta_r$) over all solid angles in the hemisphere with $\theta_r \le 90$ needs to be less than unity, with

$$\int_0^{2\pi}\int_0^{\pi/2} f_r \cos(\theta_r)\sin(\theta_r)d\theta_r d\phi = R_d + R_s \tag{6}$$

For the BRDF given in Eq. (5), this corresponds to constant values of $R_d = d\rho$ and $R_s = sF_0$. The remaining energy not reflected by the surface is either transmitted or absorbed. In this paper it is assumed the transmitted energy is zero. A review of the various BRDF models is provided in Table 1.

**Ashikhmin-Shirley**: In addition to $d$, $\rho$, and $F_0$, the Ashikhmin-Shirley BRDF has two exponential factors ($n_u$, $n_v$) that define the reflectance properties of each surface. The Ashikhmin-Shirley diffuse and specular reflectivities are not constant, however, but rather complicated functions of illumination angle, exponential factor, and the diffuse and specular reflectances. In all cases, however, $R_d + R_s \leq 1$, so energy is conserved.

**Blinn-Phong**: The specular bidirectional reflectance of the original Phong model is proportional to $\left(\hat{\mathbf{N}}\cdot\hat{\mathbf{R}}\right)^n$, where $\hat{\mathbf{R}}$ is the perfect mirror-like reflection of $\hat{\mathbf{L}}$. Blinn [20] proposes that $\hat{\mathbf{H}}$ be used instead of $\hat{\mathbf{R}}$ to make it easier and faster to calculate. Unfortunately, both versions of the model do not conserve energy and thus are unsuited for the purposes of brightness estimation. The model can be made to conserve energy, however, by modifying the leading term. In keeping with the desire for simplicity in this model, the leading term is chosen to only be a function of the exponential factor and set to yield a reflectivity equal to the mirror-like reflection of Eq. (3) at normal illumination. In addition to $d$, $\rho$, and $F_0$, the simplified Blinn-Phong BRDF has a single exponential factor ($n$) that defines the reflectance properties of each surface.

**Cook-Torrance**: This model has the facet slope distribution function ($D$), the geometrical attenuation factor ($G$) and the reflectance of a perfectly smooth surface ($F$) with $g = n^2 + (\hat{\mathbf{V}}\cdot\hat{\mathbf{H}})^2 - 1$ and the index of refraction $n = \left(1+\sqrt{F_0}\right)/\left(1-\sqrt{F_0}\right)$. In addition to $d$, $\rho$, and $F_0$, the Cook-Torrance BRDF has a facet slope ($m$) parameter that defines the reflectance properties of each surface. The facet slope parameter of the Cook-Torrance BRDF and the exponential factor of the Ashikhmin-Shirley and Blinn-Phong BRDFs are roughly related by $n = 2/m^2$.

**Table 1. Review of Various BRDF Models**

| | |
|---|---|
| Ashikhmin-Shirley | $R_d = \frac{28\rho}{23\pi}(1-sF_0)\left(1-\left(1-\frac{\hat{\mathbf{N}}\cdot\hat{\mathbf{L}}}{2}\right)^5\right)\left(1-\left(1-\frac{\hat{\mathbf{N}}\cdot\hat{\mathbf{V}}}{2}\right)^5\right)$<br>$R_s = \frac{\sqrt{(n_u+1)(n_v+1)}}{8\pi}\frac{F}{(\hat{\mathbf{V}}\cdot\hat{\mathbf{H}})\max\left[\hat{\mathbf{N}}\cdot\hat{\mathbf{L}},\hat{\mathbf{N}}\cdot\hat{\mathbf{V}}\right]}(\cos\alpha)^{n_u\cos^2\beta+n_v\sin^2\beta}$<br>$F = F_0 + \left(\frac{1}{s}-F_0\right)\left(1-\hat{\mathbf{V}}\cdot\hat{\mathbf{H}}\right)^5$ |
| Blinn-Phong | $R_d = \rho/\pi$<br>$R_s = \frac{F_0(n+2)(n+4)}{8\pi\left(n+2^{-n/2}\right)}(\cos\alpha)^n$ |
| Cook-Torrance | $R_d = \rho/\pi$<br>$R_s = \frac{DGF}{4\left(\hat{\mathbf{N}}\cdot\hat{\mathbf{L}}\right)\left(\hat{\mathbf{N}}\cdot\hat{\mathbf{V}}\right)}$<br>$D = \frac{1}{\pi m^2\cos^4\alpha}e^{-[\tan\alpha/m]^2}$<br>$G = \min\left\{1, \frac{2\left(\hat{\mathbf{N}}\cdot\hat{\mathbf{H}}\right)\left(\hat{\mathbf{N}}\cdot\hat{\mathbf{V}}\right)}{\hat{\mathbf{V}}\cdot\hat{\mathbf{H}}}, \frac{2\left(\hat{\mathbf{N}}\cdot\hat{\mathbf{H}}\right)\left(\hat{\mathbf{N}}\cdot\hat{\mathbf{L}}\right)}{\hat{\mathbf{V}}\cdot\hat{\mathbf{H}}}\right\}$<br>$F = \frac{\left(g-\hat{\mathbf{V}}\cdot\hat{\mathbf{H}}\right)^2}{2\left(g+\hat{\mathbf{V}}\cdot\hat{\mathbf{H}}\right)^2}\left\{1+\frac{\left[\hat{\mathbf{V}}\cdot\hat{\mathbf{H}}\left(g+\hat{\mathbf{V}}\cdot\hat{\mathbf{H}}\right)-1\right]^2}{\left[\hat{\mathbf{V}}\cdot\hat{\mathbf{H}}\left(g-\hat{\mathbf{V}}\cdot\hat{\mathbf{H}}\right)+1\right]^2}\right\}$ |

## 3. SOLAR RADIATION PRESSURE DEPENDENCE ON BRDF

As described in Ref. [22], in general, $R_d$ and $R_s$ are complicated functions of illumination angle and material properties represented by parameters within the particular BRDF model. For certain BRDFs, however, the integral

can be solved analytically. For example, the BRDF with a Lambertian diffuse component and purely "mirror-like" specular component (where $\hat{\mathbf{R}} = 2\left(\hat{\mathbf{L}}\cdot\hat{\mathbf{N}}\right)\hat{\mathbf{N}} - \hat{\mathbf{L}}$ is the direction of mirror-like reflection of $\hat{\mathbf{L}}$) is given by

$$f_r = d\left(\frac{\rho}{\pi}\right) + s\left(\frac{F_0\,\delta\left(\hat{\mathbf{V}} - \hat{\mathbf{R}}\right)}{\cos\theta_i}\right) \tag{7}$$

where $\delta$ is the Delta function. If the BRDF of Eq. (7) is substituted into Eq. (2), the following acceleration due to the SRP is found by

$$\mathbf{a}_{SRP} = -\sum_{k=1}^{N_{facets}} \frac{F_{sun} A_k f_k \left(\hat{\mathbf{L}}\cdot\hat{\mathbf{N}}_k\right)_+}{m_{SO} c}\left(\left(1 - s_k\left(F_0\right)_k\right)\hat{\mathbf{L}} + \left(\frac{2}{3}d_k\rho_k + 2s_k\left(F_0\right)_k\hat{\mathbf{L}}\cdot\hat{\mathbf{N}}_k\right)\hat{\mathbf{N}}_k\right) \tag{8}$$

For a more complicated BRDF, the exact solution obtained by numerically integrating Eq. (2) is different than the idealized solution obtained by Eq. (8). The numerical integration of Eq. (2) over the full hemisphere, however, is time consuming and might be prohibitive to calculate in certain applications. In this paper, correction factors for Eq. (8) from Ref. [22] are used and the acceleration is calculated in a single step by using

$$\mathbf{a}_{SRP} = -\sum_{k=1}^{N_{facets}} \frac{F_{sun} A_k f_k \left(\hat{\mathbf{L}}\cdot\hat{\mathbf{N}}_k\right)_+}{m_{SO} c}\left(\begin{array}{l}\left(1 - \left(\Delta_{s1}\right)_k s_k\left(F_0\right)_k\right)\hat{\mathbf{L}} \\ + \left(\frac{2}{3}\left(\Delta_d\right)_k d_k\rho_k + 2\left(\Delta_{s2}\right)_k s_k\left(F_0\right)_k\hat{\mathbf{L}}\cdot\hat{\mathbf{N}}_k\right)\hat{\mathbf{N}}_k\end{array}\right) \tag{9}$$

where the $\Delta$ factors depend on the illumination angle and parameters within the BRDF model. Thus, for $\Delta_d = 1$, the diffuse reflectance is Lambertian and for $\Delta_{s1} = \Delta_{s2} = 1$, the specular reflectance is mirror-like. The further these $\Delta$ factors are from unity, the greater the difference between the BRDF model and the idealized BRDF of Eq. (8).

## 4. UNSCENTED KALMAN FILTER FORMULATION

Applying the UKF structure for attitude estimation has some challenges. For instance, although three parameter sets are attitude minimal representations, they inherently have singularities. On the other hand the quaternion representation, which is a four parameter set with no singularity, has a nonlinear constraint which results in a nearly singular covariance matrix. This does not allow use of quaternions in a straightforward UKF implementation. Reference [23] overcomes these challenges by utilizing generalized Rodrigues parameters (GRPs), a three parameter set, to define the local error and quaternions to define the global attitude.

Complete explanations of the quaternion and its mapping to GRPs are provided in Refs. [24] and [25]. In the UKF implementation described in Ref. [23], the covariance matrix is interpreted as the covariance of the error GRP because for small angle errors, the error GRP is additive and the UKF structure can be used directly to compute sigma-points. The error GRP sigma points are converted to error quaternions and then to global quaternions for the propagation stage. To compute the propagated covariance the global quaternions are converted to error quaternions and then back to error GRPs. The process is then as follows: error GRP → error quaternion, error quaternion → global quaternion, global quaternion → error quaternion, and finally error quaternion → error GRP.

The estimator discussed in this work includes constrained states since the area states are constrained to be positive. To account for these constraints two methods are used. The constrained UKF method discussed in Ref. [26] is used and proxy states method discussed in Ref. [27] is used. Reference [26] incorporates the information of the constraints in the UKF algorithm by projecting sigma points and estimates onto the constraint boundary when sigma points or estimates are found outside the feasible region. Since $r \geq 0$ we have the following constraints:

$$rA \geq 0 \tag{10a}$$

$$A \geq 0 \tag{10b}$$

Then if the constraints are violated during, sampling the sigma pointing from covariance matrix, after propagation, or after the update step, the estimates and or sigma points that violate the constraints are projected onto the constraint boundary.

The proxy state method for dealing with constraints first used in Ref. [27] is based on defined unconstrained proxy values and estimating those values instead of the constrained states. To account for the constraints within the filter, unconstrained proxy values are used in the state vector and estimation filter and these proxy values are converted back to the surface parameter value when needed. Then given a constrained parameter ($a_1 : a_1 > 0$, $a_2 : 0 < a_2 < 1$) proxies $b_1$ and $b_2$ can be defined. The conversion equations to the proxy value and from the proxy value for each of the surface parameters are

$$b_1 = \ln(a_1) \quad a_1 = \exp(b_1) \tag{11a}$$

$$b_2 = \frac{1}{2}\ln\left(\frac{a_2}{1-a_2}\right) \quad a_2 = \frac{[\tanh(b_2)+1]}{2} \tag{11b}$$

Depending on the kind of state constraint either Eq. (11a) or Eq. (11b) is used.

## 5. SIMULATION RESULTS

Two simulations cases are presented: an Ashikhmin-Shirley model and a Cook-Torrance model. Both cases have the same dynamic configuration, with same initial attitude, true orbit and true angular velocity. The cases only differ in the BRDF model used to simulate and process the measurements. For the generation of data for the true model, an equatorial ground station is chosen as the site of the observer. Also, all scenarios use the same shape model which contains six sides where the areas and BRDF parameters are assumed to be the same for each side. The SO is simulated to fly in a near-geosynchronous orbit in a trajectory that is continuously lighted. This is accomplished by inclining the orbit by 30 degrees and choosing an appropriate time of the year, thereby avoiding the shadow cast by the Earth. The simulation parameters are:

- Geographic position of the ground site is 0° North, 172° West with 0 km altitude
- Initial inertial position and velocity are chosen as $\mathbf{r}^I = [-7.8931\times10^2 \quad 3.6679\times10^4 \quad 2.1184\times10^4]^T$ km
- Initial inertial velocity is chosen as $\mathbf{v}^I = [-3.0669 \quad -4.9425\times10^{-2} \quad -2.8545\times10^{-2}]^T$ km/s
- The initial time of the simulation is May 8, 2007 at 5:27:55
- Initial quaternion: $\mathbf{q}_I^B = [1/\sqrt{2} \quad 0 \quad 0 \quad 1/\sqrt{2}]^T$
- A constant rotation rate, defined as the body rate with respect to the inertial frame, represented in body coordinates, is used given by $\boldsymbol{\omega}_{B/I}^B = [0 \quad 0.00262 \quad 0]^T$ rad/s

For all simulations scenarios, measurements are produced using zero-mean white-noise error processes with standard deviation of 0.1 for magnitude and standard deviation of 1 arc-seconds for azimuth and elevation. The initial errors for the states are 10-30 deg for all three attitudes, 14 deg/hr for the rotational rates, 100 km and 1 km/s for the position and the velocity errors, respectively, 600 kg for mass, and 0.1 for both the diffuse reflectance and specular reflectance. The initial condition error-covariance values are set to $(6.67)^2$ deg$^2$ for all three attitude components, $24^2$ (deg/hr)$^2$ for the rotational rates, and $100^2$ km$^2$ and $1^2$ (km/s)$^2$ for the position and the velocity errors, respectively. The initial condition error-covariance values for the mass, diffuse reflectance and specular reflectance are $300^2$ kg$^2$, $0.2^2$, and $0.2^2$, respectively. The time interval between the measurements is set to 30 seconds. Data is simulated for 20 nights (about 20 orbits) where observations of the SO are made each night for 1 hour. The simulation results are plotted versus number of data samples since there are large time gaps between each 1 hour data arc.

For the development of the measured light curve data a six sided facet SO shape model is used. The three parameters for the shape model are given, $l$, $a$, and $d$ which are the length, width, and height respectively, as shown in Figure 1(b). For the truth model a six-facet rectangular shape model is used with dimension $l$ = 4 m, $a$ = 2 m and $d$ = 8 m. The mass for the true SO is selected to be $m$ = 600 kg, which gives a maximum area-to-mass ratio of 0.09 for this model.

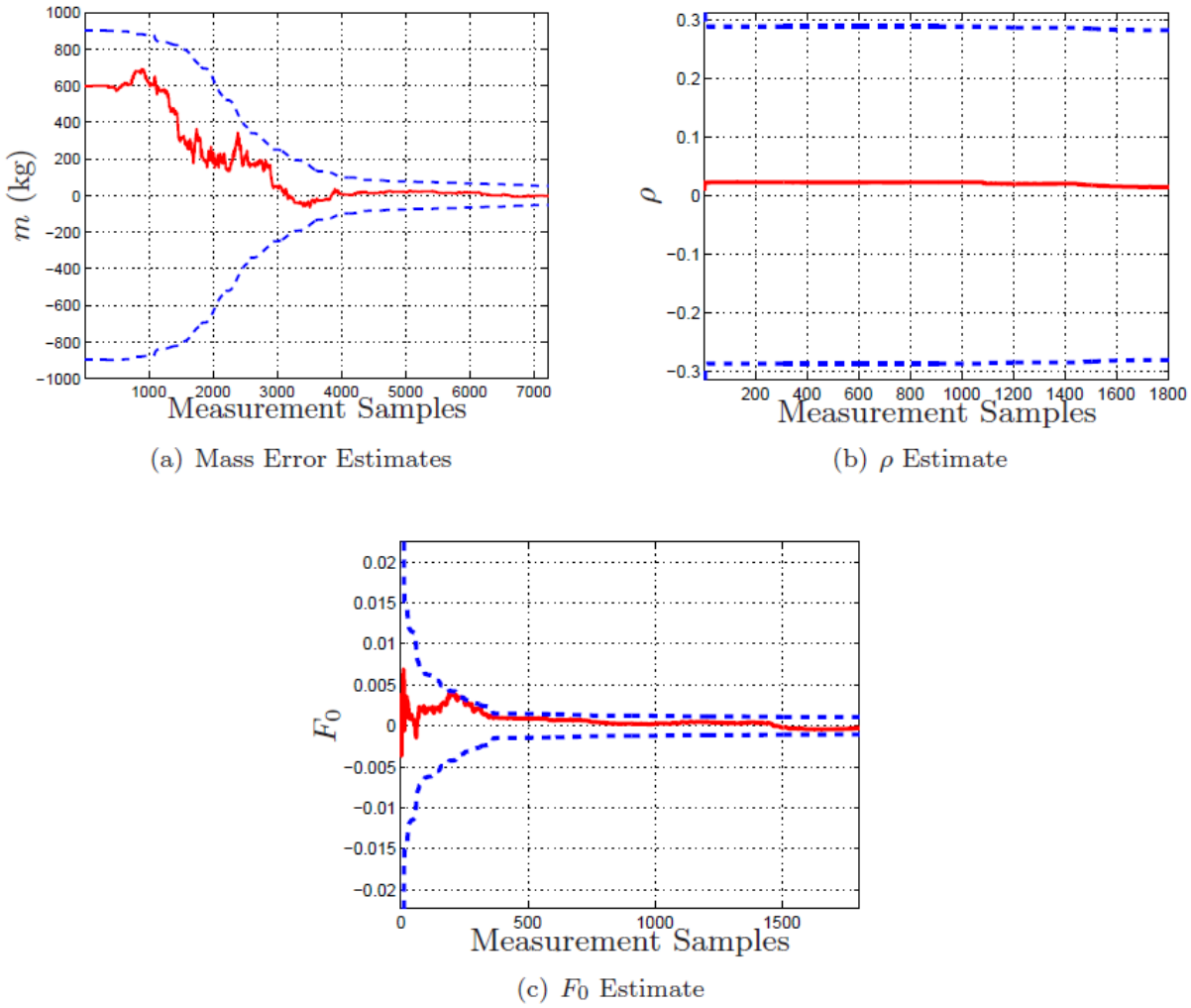


(a) Mass Error Estimates

(b) $\rho$ Estimate

(c) $F_0$ Estimate

**Figure 2. Ashikhmin-Shirley Results**

The Ashikhmin-Shirley and the Cook-Torrance model mass estimation results are shown Figs. 2 and 3. The mass estimates along with the surface parameter estimates are also shown in Figs. 2 and 3. From these figures it can be seen that the surface parameters are estimated well for both models but the parameter $\rho$ does not show good observability. This is due to the fact that truth surface parameters used are not very specular and therefore the measurements do not provide good observability with respect to $\rho$. From these figures it can also be seen that the Cook-Torrance model mass estimates coverages faster than that of the Ashikhmin-Shirley model. This can be attributed to the fact that the SRP acceleration calculated from the Cook-Torrance is larger then that of the Ashikhmin-Shirley model.

## 6. CONCLUSIONS

In this paper, an unscented Kalman filter estimation scheme using light curve and angles data was presented and was used to estimate mass and bidirectional reflectance distribution function (BRDF) parameters of a space object (SO) along with its associated rotational and translational states. This work extends previous work by using physical consistent solar radiation pressure models based on BRDFs. These models allow for fusion of light curve and angles data where the parameters used in both models are consistent and therefore provide realistic estimates. This work uses an assumed shape model of six sides and estimated the area and BRDF parameters. Both the Ashikhmin-Shirley and the Cook-Torrance BRDF models were used to simulate and process the light curve and angle measurements. Each model was used to estimate mass along with the other aforementioned states, and good performance was shown. Using an unscented filter to employ brightness magnitude and angles data, the estimator was able to determine the mass of a SO to within high accuracy.

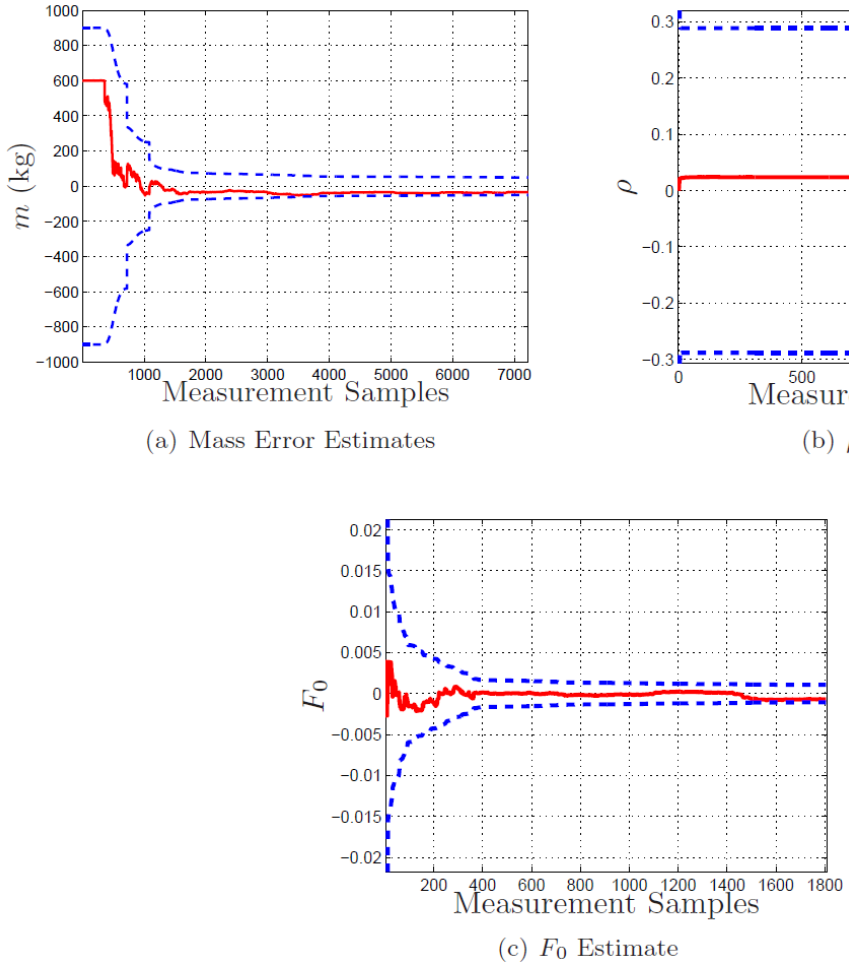


(a) Mass Error Estimates

(b) $\rho$ Estimate

(c) $F_0$ Estimate

**Figure 3. Cook-Torrance Results**

## 7. ACKNOWLEDGEMENTS

This work is sponsored by a Small Business Innovative Research (SBIR) contract FA9453-11-C-0154 by the Air Force Research Laboratory (AFRL) at Kirtland Air Force Base. The authors also wish to acknowledge useful discussions and technical contributions made by other members of the SBIR team: Paul Cefola of University at Buffalo, and Channing Chow of Pacific Defense Solutions, LLC.

## 8. REFERENCES

[1] Schildknecht, T., "Optical Surveys for Space Debris," *Astronomy and Astrophysics Review*, Vol. 14, 2007, pp. 41–111.

[2] Maruskin, J. M., Scheeres, D. J., and Alfriend, K. T., "Correlation of Optical Observations of Objects in Earth Orbit," *Journal of Guidance Control and Dynamics*, Vol. 32, 2009, pp. 194–209.

[3] Abercromby, K. J., Seitzer, P., Rodriguez, H. M., Barker, E. S., and Matney, M. J., "Survey and Chase: A New Method of Observations for the Michigan Orbital DEbris Survey Telescope (MODEST)," *Acta Astronautica*, Vol. 65, 2009, pp. 103–111.

[4] Jorgensen, K. M., Using Reflectance Spectroscopy to Determine Material Type of Orbital Debris, Ph.D. thesis, University of Colorado, May 2000.

[5] Seitzer, P., Cowardin, H. M., Barker, E., Abercromby, K. J., Foreman, G., and Horstman, M., "Photometric Studies of Orbital Debris at GEO," *5th European Space Debris Conference*, Darmstadt, Germany, March–April 2009.

[6] Abercromby, K., Hamada, K., Guyote, M., Okada, J., and Barker, E., "Remote and Ground Truth Spectral Measurement Comparisons," *Proceedings of the Advanced Maui Optical and Space Surveillance Technologies Conference*, Maui, HI, Sept. 2007, Paper E42.

[7] Cowardin, H., Seitzer, P., Abercromby, K., Barker, E., and Schildknecht, T., "Characterization of Orbital Debris Photometric Properties Derived from Laboratory-Based Measurements," *Proceedings of the Advanced Maui Optical and Space Surveillance Technologies Conference*, Maui, HI, Sept. 2010.

[8] Cowardin, H., Abercromby, K., Barker, E., Seitzer, P., Mulrooney, M., and Schildknecht, T., "An Assessment of GEO Orbital Debris Photometric Properties Derived from Laboratory-Based Measurements," *Proceedings of the Advanced Maui Optical and Space Surveillance Technologies Conference*, Maui, HI, Sept. 2009, Paper E25.

[9] Papushev, P., Karavaev, Y., and Mishina, M., "Investigations of the Evolution of Optical Characteristics and Dynamics of Proper Rotation of Uncontrolled Geostationary Artificial Satellites," *Advances in Space Research*, Vol. 43, No. 9, 2009, pp. 1416–1422.

[10] Lamboura., R., Rajana, N., Morgana, T., Kupieca, I., and Stansbery, E., "Assessment of Orbital Debris Size Estimation from Radar Cross-Section Measurements," *Advances in Space Research*, Vol. 34, 2004, pp. 1013–1020.

[11] Mulrooney, M., Matney, M. J., Hejduk, M. D., and Barker, E. S., "An Investigation of Global Albedo Values," *Proceedings of the Advanced Maui Optical and Space Surveillance Technologies Conference*, Maui, HI, Sept. 2008, Paper E65.

[12] Vrba, F., Hutter, D., Shankland, P., Armstrong, J., Schmitt, H., Hindsley, R., Divittorio, M., and Benson, J., "A Survey of Geosynchronous Satellite Glints," *Advanced Maui Optical and Space Surveillance Technologies Conference*, 2009.

[13] Holzinger, M. J., Optimal Control Applications in Space Situational Awareness, Ph.D. thesis, University of Colorado, 2011.

[14] Kelecy, T. and Jah, M., "Analysis of High Area-to-Mass Ratio (HAMR) GEO Space Object Orbit Determination and Prediction Performance: Initial Strategies to Recover and Predict HAMR GEO Trajectories with No a priori Information," *Acta Astronautica*, Vol. 69, No. 7-8, Sept. 2011, pp. 551–558.

[15] Linares, R., Crassidis, J. L., Jah, M., and Kim, H., "Astrometric and Photometric Data Fusion for Orbit, Attitude, and Shape Estimation," *AIAA Guidance, Navigation and Control Conference*, Chicago, IL, Aug. 2010, AIAA-2009-6293.

[16] Nakamura, N. A. M., Astronomical, S., and Science, A., "Detection of Mass, Shape and Surface Roughness of Target Asteroid of MUSES-C by LIDAR," *Advances in Space Research*, Vol. 29, No. 8, 2002, pp. 1231–1235.

[17] Hanada, T. and Liou, J., "Theoretical and Empirical Analysis of the Average Cross-Sectional Areas of Breakup Fragments," *Advances in Space Research*, Vol. 47, No. 9, 2011, pp. 1480–1489.

[18] Linares, R., Jah, M. K., Leve, F. A., Crassidis, J. L., and Kelecy, T., "Astrometric and Photometric Data Fusion For Inactive Space Object Feature Estimation," *Proceedings of the International Astronautical Federation*, Cape Town, South Africa, Sept. 2011, Paper ID: 11340.

[19] Ashikmin, M. and Shirley, P., "An Anisotropic Phong Light Reflection Model," Tech. Rep. UUCS-00- 014, University of Utah, Salt Lake City, UT, 2000.

[20] Blinn, J. F., "Models of Light Reflection for Computer Synthesized Pictures," *SIGGRAPH '77: Proceedings of the 4th Annual Conference on Computer Graphics and Interactive Techniques*, San Jose, CA, June 1977, pp. 192–198.

[21] Cook, R. L. and Torrance, K. E., "A Reflectance Model for Computer Graphics," *ACM Transactions on Graphics*, Vol. 1, No. 1, Jan. 1982, pp. 7–24.

[22] Wetterer, C. J., Linares, R., Crassidis, J. L., Kelecy, T. M., Ziebart, M. K., Jah, M. K., and Cefola, P. J., "Refining Space Object Radiation Pressure Modeling with Bidirectional Reflectance Distribution Functions," accepted to the *Journal of Guidance, Control, and Dynamics*.

[23] Crassidis, J. L. and Markley, F. L., "Unscented Filtering for Spacecraft Attitude Estimation," *Journal of Guidance, Control and Dynamics*, Vol. 26, No. 4, July-Aug. 2003, pp. 536–542.

[24] Shuster, M. D., "A Survey of Attitude Representations," *Journal of the Astronautical Sciences*, Vol. 41, No. 4, Oct.-Dec. 1993, pp. 439–517.

[25] Schaub, H. and Junkins, J. L., "Stereographic Orientation Parameters for Attitude Dynamics: A Generalization of the Rodrigues Parameters," *Journal of the Astronautical Sciences*, Vol. 44, No. 1, Jan.-March 1996, pp. 1–20.

[26] Kandepu, R., Imsland, L., and Foss, B. A., "Constrained State Estimation Using the Unscented Kalman Filter," *16th Mediterranean Conference on Control and Automation*, No. i, IEEE, Congress Centre, Ajaccio, France, June 2008, pp. 1453–1458.

[27] Wetterer, C. J., Crassidis, J. L., Linares, R., Chow, C. C., and Jah, M. K., "Simultaneous Position, Velocity, Attitude, Angular Rates, and Surface Parameter Estimation Using Astrometric and Photometric Observations," *Proceedings of the FUSION Conference*, Istanbul, Turkey, July 2013.